8th International Conference on Heat Transfer, Fluid Mechanics and Thermodynamics
11 – 13 July 2011
Pointe Aux Piments, Mauritius

COMPARISON OF MESH ADAPTATION TECHNIQUES FOR HIGH-SPEED COMPRESSIBLE FLOW PROBLEMS

THE SCRAMJET TESTCASE FOR THE EULER EQUATIONS.

R. Becker, K. Gokpi, E. Schall*, D. Trujillo

* Author for correspondance

SIAME-LMA-Concha - Bât. IPRA

Université de Pau et des Pays de l'Adour

PB 1155, 64010 Pau

France

E-mail: eric.schall@univ-pau.fr

Abstract

We consider the classical Scramjet test problem for the compressible Euler equations. Our objective is the comparison of different mesh refinement techniques: on the one hand hierarchical refinement of quadrilateral meshes with hanging nodes, on the other hand isotropic and anisotropic triangular meshes. Discretization of the Euler equations written in conservative variables is done by a standard discontinuous finite element (Galerkin) method. In each step of the algorithm, an error indicator is used to guide the mesh modification. Here we implemented as criterion for quadrilateral mesh refinement, indicators based on the physical variables jumps, as they are usually used in practice. Comparison is done with respect to the resolution of certain physical features, and also with respect to CPU-time, which appears to be fair, since the different algorithms are programmed within the same program handling the different ingredients in a uniform manner. For the anisotropic mesh refinement algorithm we use BAMG. All other algorithms have been implemented by the authors in the C++-library Concha.

1 Introduction

Over the past decades, significant advances have been made in developing the Discontinuous Galerkin Finite Element Method (DGFEM) for applications in fluid flow and heat transfer. Certain features of the method have made it attractive as an alternative to other popular methods such as finite volumes in thermal fluids engineering analyses. The DGFEM has been used successfully to solve hyperbolic systems of conservation laws [3, 4, 8, 9]. It makes use of completely discontinuous finite element spaces and an adequate variational formulation, especially imposing weak continuity at interelement boundaries. It was first introduced by Reed and Hill [17] for the solution of the neutron transport equation, and its history and recent development have been reviewed by Cockburn et al. [1, 2]. The DGFEM method has several advantages over continuous methods, since it uses completely discontinuous polynomial bases, it can sharply capture discontinuities which are common for hyperbolic problems and also can make mesh refinement easier in the presence of hanging nodes. The DGFEM has a simple communication pattern that makes it useful for parallel computations.

The development of self-adaptive mesh refinement techniques in computational fluid dynamics (CFD) is motivated by a number of factors. First of all, the physical solutions often present different types of singularities, such as shocks, internal and boundary layers, and sharp gradients due to singularities in the geometry of the computational domain. It is therefore evident that a uniform mesh refinement is not optimal to capture these features. On the other hand, finding an efficient local mesh resolution by hand is often impossible, especially for high accuracy demands and in cases where it is difficult to predict the location of the singularities, as for nonlinear shocks. Therefore, automatic mesh refinement algorithms have become necessary. One should emphasize that the gain in efficiency does not only concern CPU-time but also memory requirements, as reported in the literature [16].

The typical structure of an adaptive algorithm is the following

$$\text{Solve} \rightarrow \text{Estimate} \rightarrow \text{Mark} \rightarrow \text{Refine}. \quad (1)$$

Here, we compare two different techniques. They differ in the last two steps, the marking and refinement. In the hierarchical refinement algorithms, the marking decides whether a cell should be refined. Since certain constraints on the obtained meshes are in general required, the refinement algorithm possibly leads to refinement of additional cells. We only consider isotropic refinement, that is, all marked cells are bisected.

In the anisotropic refinement algorithm, a metric-based refinement is used [10] (more recently see [11]), which requires in the mark step the interpolation of the indicators. The two techniques differ considerably: the second one allows for very economical meshes in the case of lower-dimensional singularities, as in the case of shocks, and is therefore expected to outperform the first in terms of mesh

cells. On the other hand, the hierarchy is lost, and therefore, despite the interpolation of solutions from one mesh to the other, one might expect higher iteration numbers due to worse initial conditions. In order to analyze only one of these aspects, we also compare the metric-based anisotropic and isotropic variants.

In both cases we consider the same ingredients for discretization, iterative solution, and estimation, which is based on simple jump indicators. Although more elaborate error estimators are available in the literature, see for example [6, 7, 14, 18], we restrict ourselves to the simple indicators which are commonly used in practice, since the are identical in the case of isotropic and anisotropic refinement. We use indicators based on the *Mach number*, the *pressure*, and the *density*. We perform first of all comparison between these indicators in other to choose the accurate one which will very well capture the discontinuity phenomena which occur in the scramjet problem. Second of all, we perform a mesh refinement with our criterion on a hierarchical non conform rectangular grid compares with an isotropic and anisotropic refinement on triangular mesh refinement. Finally we compare the CPU related to the resolution of the different cases of mesh refinement.

2 Description of the numerical method

We denote by u the vector of physical variables, i.e. $u = (\rho, \rho v, \rho E)$ where ρ, v, and E are the *density*, the velocity field, and the total energy. The *pressure* is related to ρ and E by the ideal gas law. We write the system of equations as

$$u_t + \operatorname{div} f(u) = 0, \tag{2}$$

completed by a set of appropriate boundary conditions.

The discontinuous finite element method is based on a piecewise polynomial approximation over a mesh h (either triangular or quadrilateral). The set of cells of h is denoted by $\mathscr{K}_h$ and the set of interior sides by $\mathscr{S}_h$; the set of boundary sides is denoted by $\mathscr{S}_h^\partial$. In addition, we denote by T_K the transformation of a reference cell to the physical cell K (it is linear in the case of triangles and bilinear in the case of quadrilaterals) and by R^k the set of polynomials of either total or maximal degree k (P^k for triangles and Q^k for quadrilaterals). The discontinuous finite element space is then defined as

$$V_h^k := \{v_h \in L^2(\Omega) : \ v_h|_K \bullet T_K \in (R^k(K)^5 \quad \forall K \in \mathscr{K}_h\}. \tag{3}$$

The discrete variational formulation now reads: Find $u_h \in V_h$ such that for all $v_h \in V_h$:

$$a_h(u_h)(v_h) = l_h(v_h) \quad \forall v_h \in V_h, \tag{4}$$

where l_h is linear functional representing the inflow data and the form a_h is composed of three terms corresponding tho the mesh cells, interior sides, and boundary sides:

$$a_h(u_h)(v_h) = a_h^{\mathscr{K}_h}(u_h)(v_h) + a_h^{\mathscr{S}_h}(u_h)(v_h) + a_h^{\mathscr{S}_h^\partial}(u_h)(v_h). \tag{5}$$

The three terms are given by

$$\begin{aligned} a_h^{\mathscr{K}_h}(u_h)(v_h) &:= -\sum_{K\in\mathscr{K}_h}\int_K f(u_h) : \nabla v_h \, dx, \\ a_h^{\mathscr{S}_h}(u_h)(v_h) &:= \int_{\mathscr{S}_h} F(u_h, n_S)\cdot[v_h]\, ds, \\ a_h^{\mathscr{S}_h^\partial}(u_h)(v_h) &:= \int_{\mathscr{S}_h^\partial} \Phi(u, u_d, n_S)\cdot v \, ds. \end{aligned} \tag{6}$$

Here Φ and F are numerical fluxes representing the boundary conditions and the inter-element continuity. We will throughout use the HLLC-flux.

For higher-order approximation $k > 0$, it is well-known that a shock-capturing term has to be added to the formulation (4). However, these terms depend on geometrical quantities such as the diameter or measure of a cells and edges, and their analysis for anisotropic meshes is not clear nowadays. For this reason, we have decided to restrict ourselves to the case $k = 0$ in order to have a fair comparison between the isotropic and anisotropic meshes. The discrete equations are solved by a semi-implicit Euler time-scheme with a Newton-type linearization.

2.1 The refinement indicator

A posteriori estimates of the discretization errors use the computed solution to enhance accuracy. There exist works on the adaptive processes based on error estimates dealing with hyperbolic problems [14, 15, 12, 18]. Indicators can be constructed in many different ways. Here we use indicators which measure locally the jump of the discrete variables of the computed solutions. This error indicator is obtained by evaluating the jump (i.e. the absolute difference) of some indicator variable like the *Mach number*, *density* or *entropy* along an edge.

The main algorithmic steps then become:
- identify the elements to be refined/coarsened;
- make elements to be refined compatible by expanding the refinement region;
- make elements to be coarsened compatible by reducing the coarsening region;
- refine/coarsen the mesh;
- correct the location of new boundary points according to the surface definition data available;
- interpolate the unknowns and boundary conditions.

The aim of the identification of the elements to be refined is to determine on which sides further gridpoints need to be introduced, so that the resulting refinement patterns on an element level belong to the allowed cases listed above, thus producing a compatible, valid new mesh. Five main steps are necessary to achieve this goal:
(i) mark elements that require refinement,
(ii) add protective layers of elements to be refined,
(iii) avoid elements that become too small or that have been refined too often,

(iv) obtain preliminary list of sides where new points will be introduced,
(v) add further sides to this list until an admissible refinement pattern is achieved.

The procedure of refinement is described in the following way. One computes initially an estimator related to the jump of the physical variables. One lays out the solutions values so as to obtain a percentage of the total sum. All the elements whose values are taken into account in the quantity taken are marked. This marking is carried out on the quadrangle mesh. When the elements concerned are marked one passes at the stage of the refinement which is made of hierarchical non conform quadrangles. This new grid is interpolated for a new calculation. Let's underline that the algorithm used for the adaptive refinement can be apply to any finite volume code except particular treatment. In the adaption process, for both techniques, a solution has been computed with the background mesh. In order to transfer the solution on the new mesh generated mesh, one needs to interpolate the old solution. This transfer solution may be the good initial guess for the solution on the new mesh. This interpolation is carried out in a P^1 Lagrange context. The triangular meshes anisotropic and isotropic are constructed by the software Bamg. Bamg is a generator of isotropic or anisotropic two-dimensional grids. It allows to build a grid starting from a geometry (a border) or to build a grid adapted on the basis of a previous grid and giving itself a solution or metric. It also allows, in this case, to interpolate on the grid created the solutions, in the case P^1, defined on the previous grid [10]. The diagram for computation and refinement can be seen in figure 1

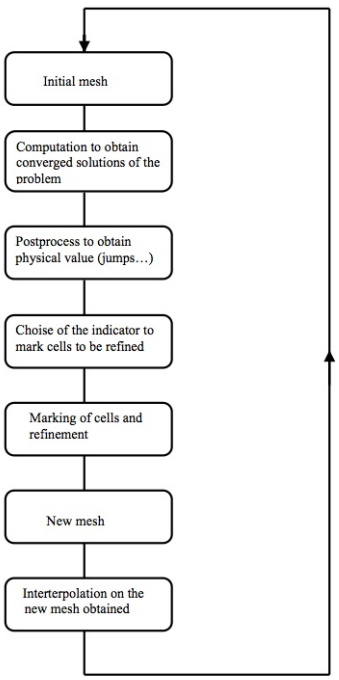

Figure 1: *Diagram of the adaptive refinement*

3 Results and discussion

In this section we consider a configuration of compressible inviscid flow. The case consists of an internal supersonic flow in a scramjet inlet. It represents a flow in convergent provided with internal obstacles representing a nozzle. The three parts of the nozzle are made up of a convergent, a throat and a divergent. Thus, the flow entering the Scramjet has the possibility of going either in the convergent ones located above and below the nozzle or to pass in it. The aim is to obtained stationary solution of air flow entering at *Mach number* 3 in atmospheric standard conditions. This configuration is chosen because it has been approved [13] and shows interesting physical phenomenon of different nature as shock-boundary layer interactions, *pressure* wave-shocks, shock-shock interactions and expansion wave-shock. We will discuss the choice of the indicator for the adaptive mesh refinement in the case of the quadrangle grids; and we'll compare this refinement to the anisotropic and isotropic ones.

3.1 Importance and influence of indicator

We recall that the purpose of adaptive refinement is to capture physical phenomenon in certain regions of the flow in order to achieve accuracy of the solution of the problem considered. For this purpose we propose to compare different kind of indicator based on the calculations of the jumps. We test different indicators: (*Rho* (R), *pressure* (P), *Temperature* (T), *Mach number* (M)), over an initial mesh Quad0 for quadrangles. The criterion retained for the refinement is the jump of the indicator selected. One respectively names Quad1_rho, Quad1_pressure, Quad1_temperature and Quad1_Mach, the various grids obtained after refinement according to indicators *rho*, *pressure*, *temperature* and the *Mach number*. The results obtained for the number of cells and vertices are shown in the following table 1.

Quadrangles	Vertices	Cells
Quad0	1175	1040
Quad1_rho	3023	2708
Quad1_pressure	3060	2738
Quad1_temperature	3405	3062
Quad_Mach	3425	3083

Table 1: *Comparison of refinement according to the various indicators*

Globally, it is observed that refinements are almost identical for the indicators R and P and for T and M. However, one notes a better space distribution of refinement for the grids , showing a better capture of physical phenomena (Figure 2).

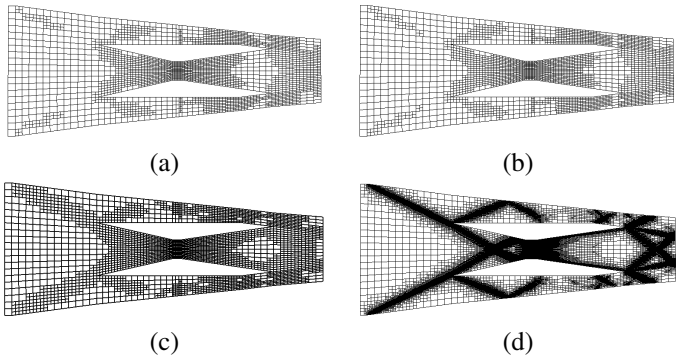

Figure 2: *Adaptive mesh refinement with the various indicators (a) Rho jump (b) Pressure jump (c) Temperature jump (d) Mach number jump*

The following figure (figure3a) compares the grids obtained at the end of the fourth iteration by superimposing them, using two type of indicators. The mesh refinement according to the *Mach number* in red is found in background and *Rho* ones in black in the foreground. One notices that refinement according to the *Mach number* seems to cover a wider area, in particular in capturing shocks. However if we invert the superposition of the grids as well as the colors, it is the *density* which seems to be well adapted because it covers a broader field. (figure 3b).

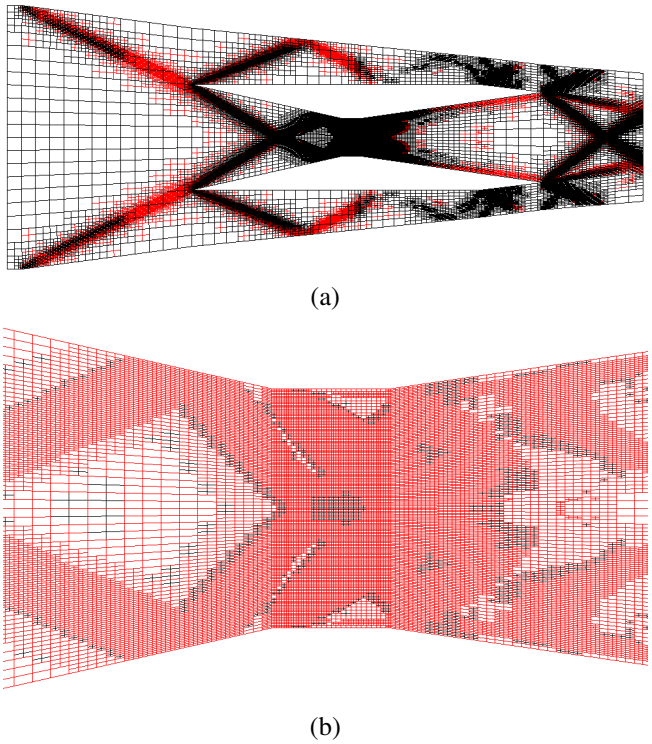

Figure 3: *(a) Superposition of the fourth iteration refinement of Rho and Mach number (b) Zoom*

In figure 4, one superposes the grid obtained after the first refinement (red) and the one obtained after the fourth refinement iteration (black) with *density* jump as estimator. These grids are perfectly encased because of the hierarchical technique of refinement. It is interesting to note that the first refinement strongly influences the successive zones of refinement. In fact the zones which are not taken into account in the first refinement are not any further during next mesh-refinement iterations. The choice of the indicator such as defined as well as the first refinement is of a paramount nature in the capture of the observable physical phenomena.

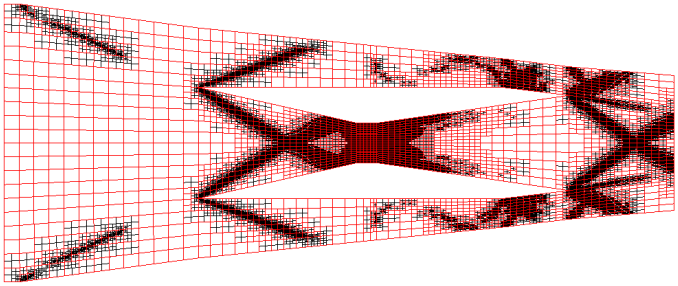

Figure 4: *Superposition of the first and the fourth iteration refinement with the indicator Rho*

We choose for the the continuation of the study the jump of the *Mach number* as estimator of the mesh refinement in the case of quadrangles since it well covers the physical phenomena in the totality of the domain.

3.2 Comparison of the techniques of refinement between anisotropic-isotropic triangles and quadrangles grids

Mesh_test	Vertices	Cells	Segments	Time/iter
Tri0	932	1594	2527	0.1918
Tri_iso1	1733	3153	4887	1.0754
Tri_iso2	4744	9040	13785	2.6138
Tri_iso3	12232	23891	36124	5.2462
Tri_iso4	32498	64303	96802	205.02
Tri_aniso1	1728	3126	4855	4.3012
Tri_aniso2	4663	8827	13491	4.7201
Tri_aniso3	12328	23960	36289	25.2993
Tri_aniso4	32366	63848	96215	462.452
Quad0	1175	1040	2216	0.1255
Quad1	3425	3083	6774	0.3375
Quad2	9709	8915	19576	0.8744
Quad3	26339	24500	53666	1.8454
Quad4	67766	63599	13827	7.9614

Table 2: *Comparison of refinement of anisotropic-isotropic and non conform quadrangles grids*

We choose to perform four successive refinements according to algorithm described in the previous section. Being given that the method of resolution is based on finite elements method, one asserts as constraint to roughly preserve the same number of cells at each stage of refinement. This in order to be able to compare in particular the computing times

per iteration. The computation is stopped when the convergence of stationary state is reached.
Three types of refinement are tested: An anisotropic and isotropic refinement for triangles on one hand and on the other an hierarchical non conform refinement for quadrangles. For the three cases, the following constraints are asserted :

-The indicator retained is the jump of the *Mach number*
-The time step is constant and equal to $10^{-3}s$
-The convergence is obtained after approximately 90 to 95 iterations

3.2.1 Interest and Influence of refinement: example of isotropic triangles case

The Figure 5 represents the evolution of the *density* along axis of symmetry of the nozzle for the four cases of the mesh refinement (Tri_iso1 to Tri_iso4)

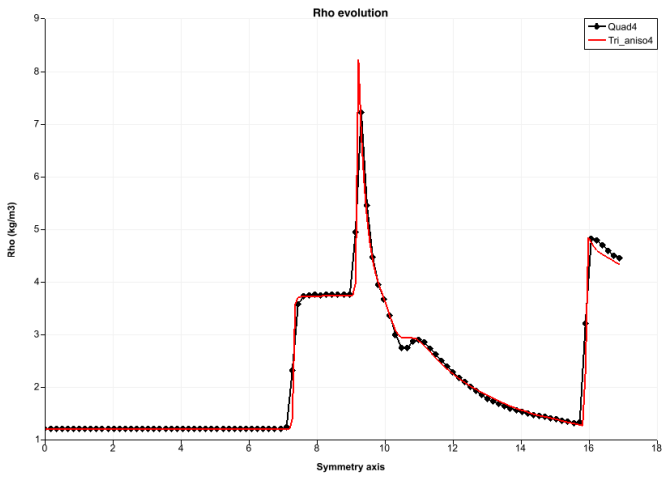

Figure 5: *Evolution of density along symmetry axis for isotropic mesh refinement*

One observes two zones of very strong compression. The first one at $x-coordinate$ 7, relating to the interaction of the two oblique shock waves resulting from the leading edges of the two obstacles symmetrically opposite. The second one is relative to a small fragment of right shock wave located at $x-coordinate$ 9.3 approximatively in the center of the nozzle throat. At immediate downstream of the latter, the subsonic shocked flow undergoes the process of expansion or acceleration of the fluid expected in the divergent of the nozzle.
The capture of the physical phenomena is of as much better than the grid contains elements (or nodes) where the gradients are most important . The adaptive mesh refinement shows here all its interest. The Tri_iso4 grid gives, obviously, the best result with steep slopes on the level of shocks and a plate well represented between the first shock ($x-coordinate$ 7.3) and the right shock ($x-coordinate$ 9.2). However, One notes a relative difference in evolution of the expansion in case Tri_iso4 compared to the three other first cases. In fact, it appears a point of inflection at the level of the decrease of the *density* at the $x-coordinate$ 10.8 approximately . We will reconsider this difference in what follows.

3.2.2 Comparison between anisotropic and isotropic grids

Let's now compare, the results obtained on the cases of the fourth mesh refinement in triangles isotropic (Tri_iso4) and anisotropic (Tri_aniso4). Figure 6

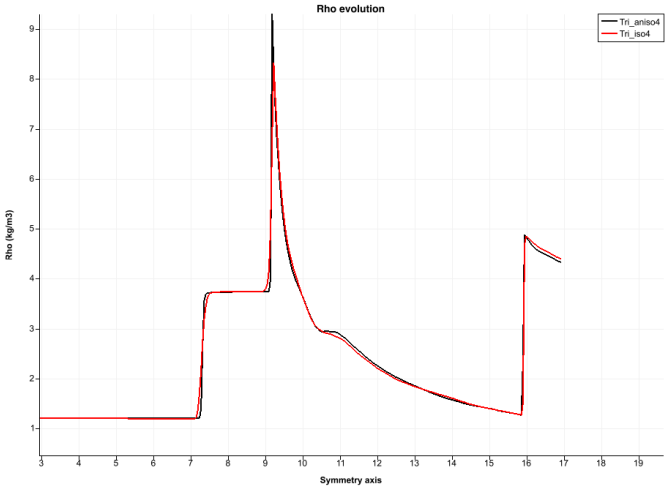

Figure 6: *Comparison between anisotropic and isotropic mesh refinement*

The gradients obtained on the figure 6 are even stiffer with the anisotropic case and the capture of the peak of *density* continues to go up. It is also noticed that the phenomenon of inflection point observed previously is still accentuated with the appearance of a kind of plate.

In conclusion to this part, we retain that the anisotropic grids give better results than those obtained by the isotropic grids as for the capture of the physical phenomena observed.

3.2.3 Technics comparison of adaptive mesh refinement in triangles and quadrangles

The following figures represent the grids obtained after the fourth refinement iteration for the anisotropic triangles (Tri_aniso4) and the quadrangles (Quad4). (see figures 7a, 7b).

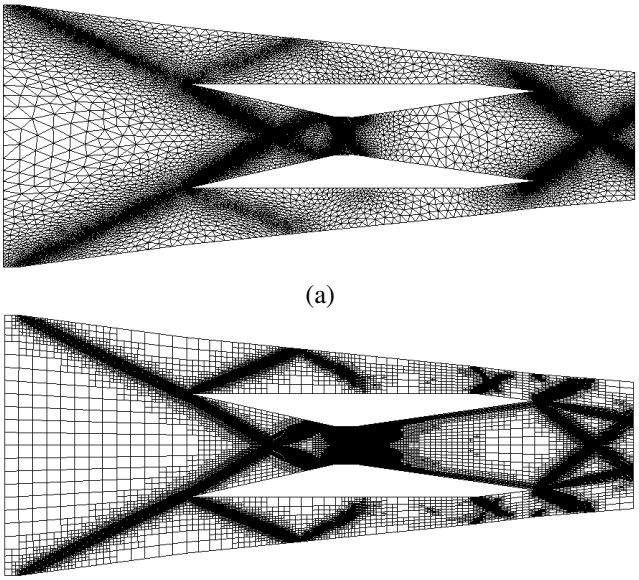

(a)

(b)

Figure 7: *(a) Anisotropic mesh refinement iteration on triangles (fourth mesh refinement iteration) (b) Hierarchical non conform mesh refinement iteration on quadrangles (fourth mesh refinement iteration)*

The figure (8) shows two results relatively surprising. In fact, the anisotropic triangles mesh captures well the shocks (more stiffness in the curve and a maximum value of the higher *density*). On the other hand, it would seem that the grid in quadrangles collects an additional physical phenomena at the expansion in divergent of the nozzle.
In fact, the monotonous decrease observed on the previous figures (6, 7) is broken by a break of slope before decreasing again.

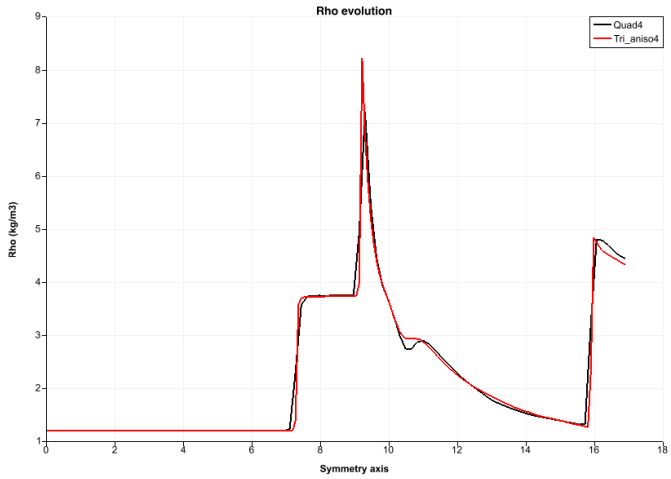

Figure 8: *Comparison of the evolution of density between anisotropic triangles and hierarchical non conform mesh refinement*

One realizes better this break of slope on the figure of the Iso-values of the *density* by zooming in the divergent part of the nozzle when adjusting the colors values scale as shown in figures 9.

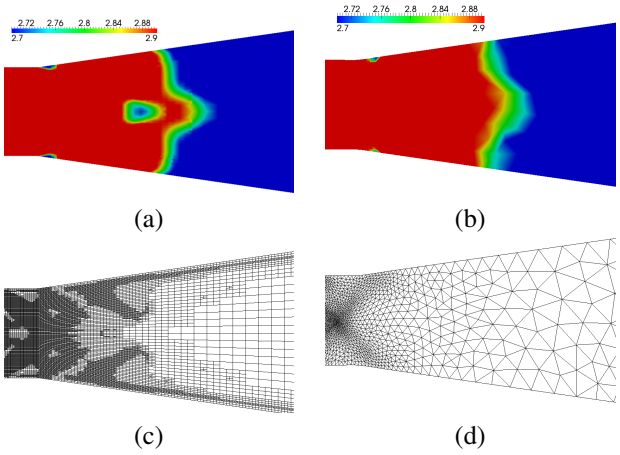

(a) (b)

(c) (d)

Figure 9: *(a) Density iso-values at the downstream of the divergent of the nozzle (Quad4) (b)Density Iso-values at the downstream of the divergent of the nozzle (Tri_aniso4) (c) Corresponding mesh to (a), (d) Corresponding mesh to (b)*

These figures of mesh refinement in the two cases, shows that the *density* of mesh is more important for the grid in quadrangles than those in triangles.

3.3 Comparison of the computing time

The figures below represent the average computing times per iteration obtained for the three types of mesh refinement represented in table 2. From this table we can make the following remarks:
- It takes approximately twice more time to obtain a calculation using an anisotropic grid compared to an isotropic ones. (see Figures 10 and table 2)
- The computing times obtained with the grids in quadrangles follow approximatively a linear progression while those obtained with the triangles grids increase in a cubic way. In fact, the converged solution obtained with Quad4 is at least 68 times faster than that of Tri_aniso4. Moreover, it is noted that it was necessary to divide the time step by 10 with the anisotropic triangles computation from the third refinement to be able to converge to the stationary state.

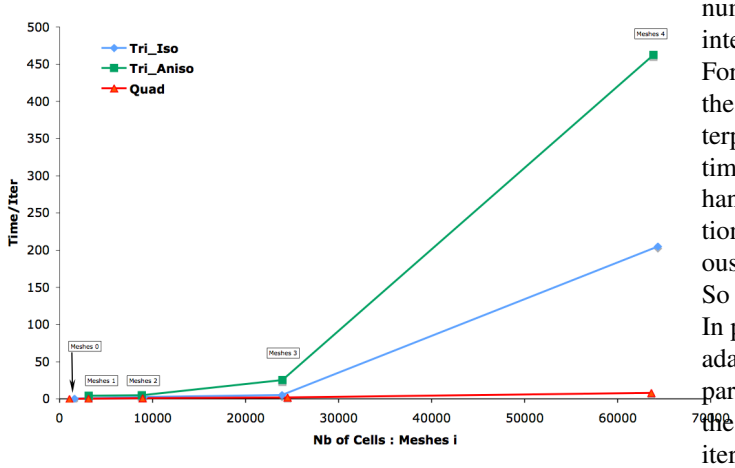

(a)

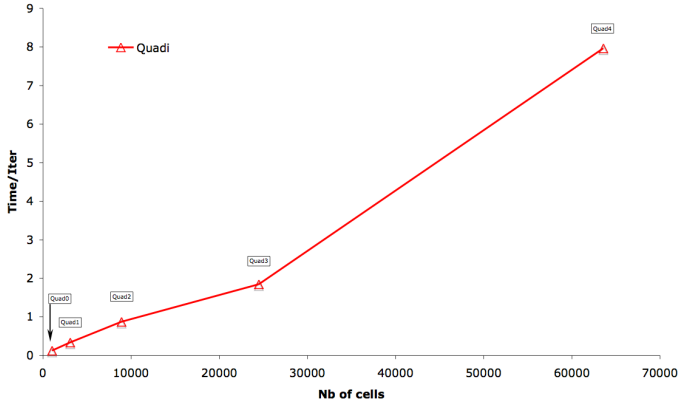

(b)

Figure 10: *(a) Computing times of the three cases of mesh refinement (b) Computing time of mesh refinement with quadrangles*

4 Conclusion and perspectives

We developed a discontinuous Galerkin finite element method resolution to solve Euler equations. The Galerkin finite element method has several advantages, and one of them is the interelement discontinuity as criteria of a posteriori error estimation for an adaptive algorithm for mesh refinement. The case of scramjet is chosen due to the complexity of the phenomenon of waves interactions. The results we presented show many features concerning the choice of the indicators. They can capture adequately the physical phenomenon in a fluid flow especially in the case of many interactions such as shock-shock, shock-wall. We used two techniques of adaptive mesh refinement: isotropic or anisotropic for triangles with Bamg software and hierarchical non conform for quadrangles whom we implemented ourselves.
The advantage of mesh refinement with triangles is that between two mesh refinements, most of the mesh elements are in the strong gradients zones and disappear from where the gradients are weak. Approximately the zones of weak gradients are reduced in aid of zones of strong gradients where the number of elements increases. The disadvantage is that the interpolation P^1 of the solution is non-conservative.
For the quadrangular mesh refinement based on the jump of the *Mach number* as indicator, the advantage is that the interpolation of the solution is conservative and the computing times are much faster than for the triangle ones. On the other hand the disadvantage consist in the hierarchical interpolation; at a new iteration, the totality of the cells on the previous grid is conserved whatever the value of the gradients are. So the number of cells becomes more important.
In perspectives many different ways can be investigated with adaptive non conform mesh refinement with quadrangles. In particular, we plan to enhance this criteria in order to improve the adaptive mesh refinement on multi-grids with the use of iterative solvers.

Acknowledgements

Part of this research is supported by public finance of the "Direction Générale de la Compétitivité de l'Industrie" (D.G.C.I.S.) through the OPTIMAL research program, recognized by the three French aeronautical poles of competitiveness (Aerospace Valley, ASTech Paris-Area and Pôle PEGASE).

References

[1] *F. Bassi, S. Rebay, A high-order accurate discontinuous finite element method for the numerical solution of the compressible Navier Stokes equations, J. Computat. Phys. 131 (1997) 267-279.*

[2] *C.E. Baumann, J.T. Oden, A discontinuous hp finite element method for convection-diffusion problems, Comput. Methods Appl. Mech. Engrg. 175 (1999) 311-341.*

[3] *K.S. Bey, J.T. Oden, hp-version discontinuous Galerkin method for hyperbolic conservation laws, Comput. Methods Appl. Mech. Engrg. 133 (1996) 259-286.*

[4] *R. Biswas, K. Devine, J.E. Flaherty, Parallel adaptive finite element methods for conservation laws, Appl. Numer. Math. 14 (1994) 255-284.*

[5] *M. J. Castro-Diaz, F. Hecht, B. Mohammadi, New Progress in anisotropic grid adaptation for inviscid and viscous flows simulations*

[6] *B. Cockburn, A simple introduction to error estimation for nonlinear hyperbolic conservation laws, in: Proceedings of the 1998 EPSRC Summer School in Numerical Analysis, SSCM, Graduate Students Guide for Numerical Analysis, vol. 26, Springer, Berlin, 1999, pp. 146.*

[7] *B. Cockburn, P.A. Gremaud, Error estimates for finite element methods for nonlinear conservation laws, SIAM J. Numer. Anal. 33 (1996) 522-554.*

[8] *B. Cockburn, C.W. Shu, TVB Runge Kutta local projection discontinuous Galerkin methods for scalar conservation laws II: General framework, Math. Computat. 52 (1989) 411-435.*

[9] *K.D. Devine, J.E. Flaherty, Parallel adaptive hp-refinement techniques for conservation laws, Comput. Methods Appl. Mech. Engrg. 20 (1996) 367-386.*

[10] *F. Hecht, Bamg: Bidimensional Anisotropic Mesh Generator, draft version v0.58, October 1998*

[11] *A. Loseille, A. Dervieux, F. Alauzet, Fully anisotropic goal-oriented mesh adaptation for 3D steady Euler equations, Journal of Computational Physics, 229 (2010) 2866-2897.*

[12] *P. Houston, E. Süli, C. Schwab, Stabilized hp-finite element methods for hyperbolic problems, SIAM J. Numer. Anal. 37 (6) (2001) 1618-1643.*

[13] *D. Kuzmin, M. Möller, Algebraic Flux Correction II. Compressible Euler Equations , In: D. Kuzmin, R. Löhner and S. Turek (eds.) Flux-Corrected Transport: Principles, Algorithms, and Applications. Springer, 207-250, (2005).*

[14] *M. Larson, T. Barth, A posteriori error estimation for adaptive discontinuous Galerkin approximation of hyperbolic systems, in: B. Cockburn, G.E. Karniadakis, C.W. Shu (Eds.), Proceedings of the International Symposium on Discontinuous Galerkin Methods Theory, Computation and Applications, Springer, Berlin, 2000.*

[15] *E. Süli, A posteriori error analysis and adaptivity for finite element approximations of hyperbolic problems, in: D. Kroner, M. Ohlberger, C. Rhode (Eds.), An Introduction to Recent Developments in Theory and Numerics for Conservation Laws, Lecture Notes in Computational Science and Engineering, Vol. 5, Springer, Berlin, 1999, pp. 123-194.*

[16] *R. Löhner, Applied Computational Fluid Dynamics Techniques: An Introduction Based on Finite Element Methods, Second Edition, 2008, John Wiley and Sons, Ltd.*

[17] *W.H. Reed, T.R. Hill, Triangular mesh methods for the neutron transport equation, Technical Report LA-UR-73-479, Los Alamos Scientific Laboratory, Los Alamos, 1973.*

[18] *R. Hartmann and P. Houston, Adaptive discontinuous Galerkin finite element methods for the compressible Euler equations, J. Comput. Phys. 183(2) (2002) 508-532.*